Available online at www.sciencedirect.com
SCIENCE DIRECT®
Journal of Nuclear Materials 341 (2005) 83–89
journal of nuclear materials
www.elsevier.com/locate/jnucmat

Microstructural examination of V–(Fe or Cr)–Ti alloys after thermal-creep or irradiation-creep tests

K. Fukumoto *, S. Takahashi [a], R.J. Kurtz [b], D.L. Smith [c], H. Matsui [a]

[a] *Institute for Materials Research, Tohoku University, Sendai 980-8577, Japan*
[b] *Pacific Northwest National Laboratory, Richland, WA 99352, USA*
[c] *Argonne National Laboratory, IL 60439, USA*

Received 22 March 2004; accepted 17 January 2005

Abstract

Microstructural examinations have been performed on irradiation-creep and thermal-creep pressurized tube specimens of V–3Fe–4Ti–0.1Si in order to understand failure and creep mechanisms. There are no typical microstructural differences between unstressed and pressurized creep tube specimens irradiated in ATR-A1 in the irradiation temperature regime from 212 to 300 °C. Failed thermal creep specimens show dislocation structures dependent on the tube specimen geometry. This can be interpreted in terms of a large number of slip dislocations oriented for optimum slip.

PACS: 61.72.Hh; 61.80.Hg; 62.20.Hg

1. Introduction

Since vanadium alloys are candidate materials for fusion reactor structural materials, particularly because of their potentially high service temperatures, it is necessary to assess the performance of vanadium alloys at high temperature regime from 700 to 800 °C [1]. However information on the creep properties of vanadium and vanadium alloys is limited since only a few studies have been performed.

On the other hand, irradiation creep is one of important research and development issues for first wall and blanket structures of fusion reactor materials. The effect of irradiation on creep properties has been investigated and a pressurized creep tube technique has been mostly employed for in-pile creep tests [2]. A study of biaxial thermal creep properties of V–Cr–Ti alloys has been performed successfully using pressurized creep tube techniques [3]. In the ATR-A1 irradiation in the JUPITER program [4], a study of biaxial irradiation creep properties of V–Cr–Ti alloys has been performed and data of a significant irradiation creep rate were obtained [5,6]. However information on the microstructure of thermal and irradiation creep in vanadium alloys have not been reported so far. It is necessary to obtain reliable microstructures in creep deformation in order to clarify the mechanism of thermal creep and irradiation creep

* Corresponding author. Address: School of Nuclear Power and Energy Safety Engineering, University of Fukui, 3-9-1, Bunkyo, Fukui 910-8507, Japan. Tel./fax: +81 776 27 9712.
E-mail address: fukumoto@mech.fukui-u.ac.jp (K. Fukumoto).

0022-3115/$ - see front matter
doi:10.1016/j.jnucmat.2005.01.016

behavior. In this study, a vanadium alloy of V–3Fe–4Ti–0.1Si (Heat number VM9502) was used, subjected to both thermal and irradiation creep tests as in V–Cr–Ti alloy [2] and creep data were also obtained. It has been pointed out that Fe included in vanadium alloy combines with helium strongly during neutron irradiation and suggested that V–Fe–Ti alloy will show high resistance to void swelling and intergranular degradation by helium implantation at high temperatures [7]. The V–Fe–Ti alloy is considered to be superior creep strength at high temperature to the V–Cr–Ti alloy, because it has larger binding energy with He/vacancy complex cluster than the V–Cr–Ti alloy. It has been reported that the mechanical properties of the V–Fe–Ti alloys are not so much different from that of the V–Cr–Ti alloys in out-pile and in-pile irradiation conditions [6,8,9]. The purpose of this study is to clarify the relationship between microstructures and creep behavior through transmission electron microscope (TEM) observations on thermal and irradiation creep specimens.

2. Experimental procedure

2.1. Biaxial thermal creep tests

The chemical composition of the V–3Fe–4Ti–0.1Si alloy has been already reported [6]. Detailed descriptions of the creep pressurized tube specimen preparation and the experimental environment are reported in Refs [5,6,9,10]. The creep specimens in the ATR-A1 experiments and thermal creep test in Pacific Northwest National Laboratory (PNNL) were pressurized tubes with welded end plugs. The tubes were prepared from the V–3Fe–4Ti–0.1Si laboratory heat produced at Tohoku University in Japan. The tubes of V–3Fe–4Ti–0.1Si alloys were produced by machining in Argonne National Laboratory (ANL). All specimens had a nominal 4.57 mm outer diameter (OD), 0.25 mm wall thickness, and 25.4 mm length. The machining tubing was inspected with available ultrasonic or eddy current methods and radiography. Tube sections with questionable mass densities were excluded.

In order to fabricate creep tubes, the circumferential plug-to-tube welds were made with an electron-beam welder in vacuum. After the end plugs were attached, the assemblies were annealed at 1000 °C for 1.0 h in vacuum while wrapped in a Ti getter foil. They were then pressurized to the desired level, through a 0.25-mm diameter hole in the top end plug, with high-purity helium in a pressure chamber. Two of the unpressurized #832665 specimens were designated as stress-free swelling controls. The final closure weld of the 0.25 mm diameter of hole was made with a helium gas enclosure machine in ANL. The specified pressure loading was determined with a code that accounted for thermal expansion of the vanadium alloy tubing, compressibility of the helium gas, and anticipated specimen temperature. Following the leak check and visual inspection, the dimensions of the assembled creep specimens were measured with a laser profilometer. The measurements were made at five axial locations (x/l of 0.1, 0.3, 0.5, 0.7, and 0.9) at every 9° azimuthal interval, and the 19 azimuthal readings were averaged to yield the mean diameter for each axial location of the specimens.

Thermal creep experiments were performed in PNNL [3]. Prior to insertion into the vacuum furnace, each specimen was loosely wrapped with titanium foil to provide additional protection against oxygen pickup during the experiment. The specimen OD was again measured using a laser profilometer to determine the elastic diametral displacements for each tube. For creep tests of the V–3Fe–4Ti–0.1Si alloys, two test temperatures were selected, 700 and 800 °C.

Conventional analyses of grain boundary microstructure of an unstressed tube and a sample after creep test were performed by using a scanning electron microscope equipped with electron back scattering diffraction and orientation imaging microscope system (SEM–EBSP/OIM).

2.2. Biaxial irradiation creep tests

Detailed irradiation conditions have been reported in Refs [5,6]. The ATR-A1 experiment consisted of 15 stacked, lithium-bonded subcapsules. The 10 creep specimens were each contained in a subcapsule to preclude interactions should any one rupture unexpectedly. To reduce the atypical transmutation of V into Cr due to the reactor's thermal flux, a neutron filter made of Gadolinium was installed in each subcapsule. The duration of the irradiation was 132.9 effective-full-power days. The experiment had two target temperatures: 200 and 300 °C. However, because of the space limitation and axial flux gradient, the achieved displacement damage and specimen temperatures were not uniform, particularly for the nominally 200 °C specimens. In calculating the effective strains for V–3Fe–4Ti–0.1Si alloy specimens the averaged diameters were determined with the laser profilometer in the same manner as before irradiation. For the unstressed specimens for the 200 and 300 °C groups, the diametral strains of V–4Cr–4Ti alloys (the #832665-heat specimens) were used as that of the unstressed specimens for V–3Fe–4Ti–0.1Si alloys [5].

2.3. Preparation of TEM specimens and TEM observation

Ring sections of creep tubes were sectioned and cut into 2 mm^2 plates by a multi wire-saw for thermal creep tubes and by an electrical discharge machining (EDM) apparatus installed in a radiation controlled area at

Oarai branch in Institute for Materials Research/Tohoku University for irradiation creep tubes. The plate was thinned by grinding and then electro polished. No evidence of damage due to grinding could be seen in the cold-run test using an annealed and untested creep tube, therefore there were no artificial dislocations and no feature of anisotropic microstructures induced by sample preparation. TEM observations were carried out. In the TEM observation for thermal creep pressurized tube specimens, $a\,\boldsymbol{g}\cdot\boldsymbol{b}=0$ technique was performed in order to determine the Burgers vectors of dislocations. Based on the $\langle 0\,0\,1\rangle$ orientation, at least four beam injection of $\langle 0\,1\,2\rangle$ and $\langle 1\,1\,2\rangle$ directions and ten types of reflection, $\{0\,1\,1\}$, $\{0\,0\,2\}$ and $\{1\,1\,2\}$, were selected and used for each specimen. As a result, all types of $\langle 0\,0\,1\rangle$, $\langle 0\,1\,1\rangle$ and $\langle 1\,1\,1\rangle$ Burgers vector were completely distinguished.

3. Results and discussions

3.1. Microstructural examination for thermal creep pressurized tube specimens

Table 1 gives the information of thermal creep test conditions. The chemical analyses before and after thermal creep tests were carried out. An untested pressurized tube creep specimen contains 890 wppm oxygen and 80 wppm of nitrogen. On the other hand, a specimen tested at 700 °C with rupture time of 3887 h showed contents of 680 wppm oxygen and 30 wppm nitrogen. The reduction of nitrogen from V alloys during creep test could not be understood well in this study. However, it is considered that the amounts of nitrogen contents before and after creep test do not change significantly and are within the experimental errors. From the chemical analysis, any impurity incursion during the creep tests could not be recognized. Conventional analyses of grain boundary microstructure of an unstressed tube and a sample after creep test at 700 °C and 129 MPa were performed by using the SEM–EBSP/OIM system.

From the analyses of grain boundary microstructures, there were no typical differences of the grain size distribution, misorientation angle distribution and CSL (coincidence site lattice) boundaries distribution between an unstressed tube and a pressurized tube after creep test. This suggests that the grain growth, polygonization and anisotropic flow of mass transfer did not occur during the creep test at 700 °C and 129 MPa.

Fig. 1 shows a comparison of stress dependence of the minimum creep rate between the US heat 832665 of V–4Cr–4Ti alloys [3] and the V–3Fe–4Ti–0.1Si alloys. The steady-state creep regimes of strain-time curves for the V–3Fe–4Ti–0.1Si alloys were very short or not observed. In the case of no steady-state creep regimes, the first creep rates on strain-time curves were adopted as minimum creep rates. The creep rates of the V–3Fe–4Ti–0.1Si alloys were faster than V–4Cr–4Ti, #832665 alloys [3] as shown in Fig. 1. The stress exponent, n derived from a relationship between the creep rate and effective stress was 2.3 at 700 °C, which suggests that the creep mechanism is typical of solid-solution alloy. However since the steady state creep was not observed in 700 °C creep tests, the value of stress exponent is unreliable. In 800 °C creep tests, a large stress exponent of $n = 11$ was obtained, likely due to the presence of a threshold stress. Fig. 2(A) shows an example of dislocation structures in a V–3Fe–4Ti–0.1Si tested at 800 °C and 74 MPa. A lot of dislocations were formed and many precipitates were seen in grains. The dislocation structure was distributed homogeneously in grains and some dislocations were pinned at precipitates here and there. The cell walls of dislocations were seldom identified in any specimens.

On the other hand, the sub grain boundary structures, like cell walls, could be seen in a V–4Cr–4Ti alloy.

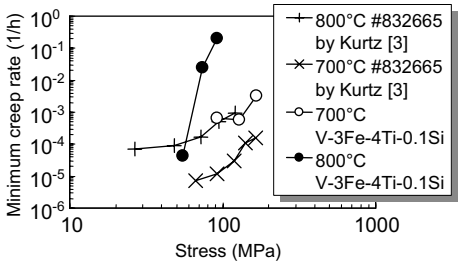

Fig. 1. Stress dependence of minimum creep rate of the US heat #832665 of V–4Cr–4Ti and the V–3Fe–4Ti–0.1Si.

Table 1
Test conditions for thermal creep pressurized tube specimens of V–Fe–Ti alloys

Temperature (°C)	Effective stress (MPa)	Time to rupture (h)	Effective mid-wall strain (%)	Minimum creep rate (%/h)
700	92	3418	15.8	6.4×10^{-4} at 101 h
	129	3887	17.3	5.7×10^{-4} at 101 h
	160	585	12.2	3.3×10^{-3} at 101 h
800	55	No rupture (till 5242)	0 at 5242 h	4.3×10^{-5}
	74	427	6.9	2.5×10^{-2}
	92	101	20.0	2.0×10^{-1} at 101 h

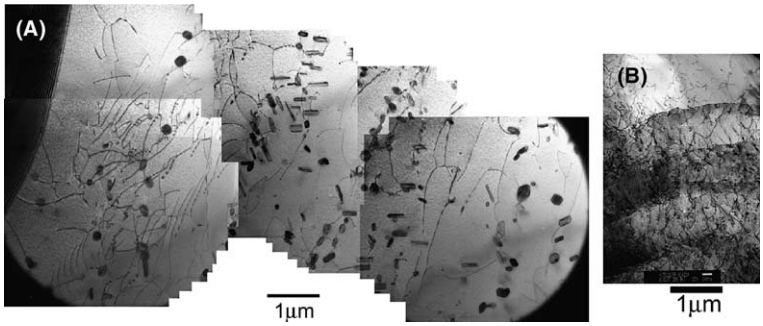

Fig. 2. Microstructures in V–3Fe–4Ti–0.1Si alloys tested at 800 °C with a stress of 74 MPa (A), and a NIFS-Heat1 tested at 800 °C with a stress of 200 MPa (B). The image (A) was taken from a failed specimen and (B) taken from a specimen ceased a creep test at the beginning of steady state creep.

A large ingot of highly purified V–4Cr–4Ti alloy, NIFS-Heat1 [11] has been examined in creep deformation test using uniaxial tensile specimens. Fig. 2(B) shows the BF images of a NIFS-Heat1 in a steady state creep regime during a creep test at 800 °C and 200 MPa using uniaxial tensile specimens [12]. Sub grains with widths of about 1 μm were distributed through grains in the NIFS-Heat1 alloy.

The difference between these alloys may be caused by the creep deformation mechanism. The type for V–3Fe–4Ti–0.1Si alloys is of the dislocation creep of solid solution alloy, and for NIFS-Heat1 alloys is of the dislocation creep of pure metal. It indicates that the dislocation glide controls the creep rate in the NIFS-Heat1 alloys, whereas solute atoms in the V–3Fe–4Ti–0.1Si alloys act as lattice resistance to dislocation motion and the glide velocity is less than the climb velocity of a dislocation.

Detailed investigation of dislocation characteristics and configuration was performed in all failed specimens. Fig. 3 shows an example of the microstructure of the V–3Fe–4Ti–0.1Si alloys tested at 800 °C and 92 MPa. Most of the dislocations had parallel alignment with the longitudinal direction of the creep tube specimens. The Burgers vector for the dislocations was $1/2\langle 1\,1\,1\rangle$. Since the direction of $\langle 1\,1\,1\rangle$ vector was perpendicular direction to dislocation line, the dislocations should be edge dislocations. The short dislocations intersecting long $\langle 1\,1\,1\rangle$ dislocations had the $\langle 1\,0\,0\rangle$ Burgers vector, which are the reaction dislocations among the different slip of

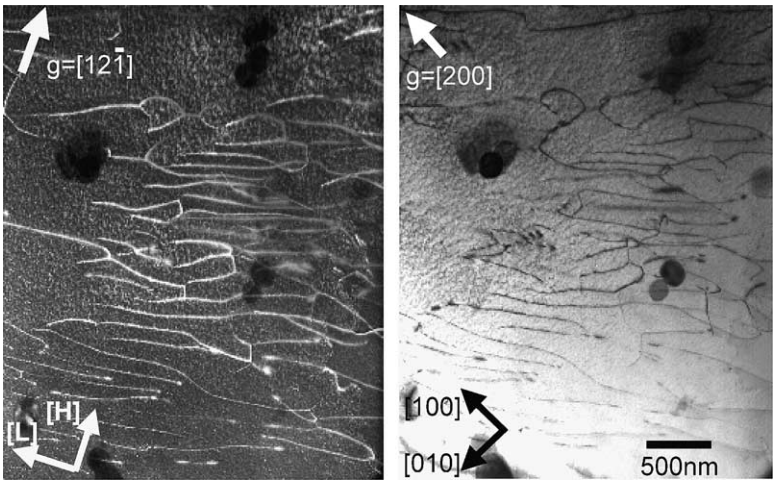

Fig. 3. Example of TEM images of a dislocation structure of the V–3Fe–4Ti–0.1Si alloy tested at 800 °C with a stress of 92 MPa. Arrows on upper part in images show the *g*-reflection vectors, $(1\,2\,\bar{1})$ for left and (0 0 2) in right. A set of arrows in the bottom of left shows the direction in pressurized creep tube geometry; [L] indicates a longitudinal direction in the tube and [H] a hoop direction. A set of arrows in the bottom of middle part shows the crystallographic directions; the projection axes is [0 0 1] direction and close to the perpendicular direction for the creep tube surface within 5°.

⟨1 1 1⟩ dislocations. Since the determination of dislocation character for many grains is difficult, the configuration of dislocations was obtained by the measurement of a direction along a dislocation line. Fig. 4 shows the plot of dislocation length distribution as a function of the angle between a longitudinal direction of creep tube and a direction along a dislocation line. A lot of long dislocations may be aligned with a longitudinal direction of creep tube at 700 °C as shown in the Fig. 4(A). On the other hand, the dislocation alignment at 800 °C is deviated from the longitudinal direction of the tubes, however most of alignment angle is concentrated within a 45ºangle from the longitudinal direction of the tubes. The deviation of angle is caused by the crystallographic geometry of each grain because the distribution of concentrated regime of dislocations is unimodal or bimodal like grain A, B and D in Fig. 4(B).

From the general stress analysis of pressurized creep tubes [5,13], a hoop stress and a longitudinal stress is described as $\sigma_\theta = (r_m/t)\Delta P$ and $\sigma_z = (0.5r_m/t)\Delta P$, respectively. The r_m is the mid-wall radii of tubes, t is the wall thickness and ΔP is the difference in internal and external gas pressure at the temperature. The direction of the main stress is the hoop direction on the pressurized creep tubes. In order to determine which slip system is dominant in creep tube deformation, trace analyses were done for the Burgers vectors of dislocations, the foil normal and the direction of the critical resolved shear stress. It is assumed that the preferential slip planes in vanadium alloys [14] are {1 1 0} or {1 1 2} and the 'easiest' slip plane was determined for each examination. Fig. 5 shows the fractional distribution for the Burgers vector of dislocations in the creep-tested V–3Fe–4Ti–0.1Si alloys. The dislocation densities of ⟨1 1 1⟩ Burgers vector were divided into two portion; the one that takes the easiest slip system and the others. Since the specimens were taken from the ruptured area in failed specimens, the dislocation densities for all specimens were almost the same, independent of the stress levels. The fraction of the ⟨1 1 1⟩ Burgers vector for the main slip is about 60–70%. It can be interpreted to contain a large number of slip dislocations oriented for optimum slip during creep tests. Multiple slip should be facilitated by geometrical effects arising from experimental constraints, but the pressurized tube is so thin that the constraint effect may not be stronger than tensile and compression tests.

In general, the mechanical properties of bcc metals and alloys are strongly dependent on temperature, strain rate, sign of stress and impurity contents. In particular, characteristic of bcc metals is the existence of two different deformation behaviors below and above a so-called transition temperature T_0, which lies somewhere between $0.1T_m$ and $0.2T_m$. The marked low temperature rise of the critical shear stress is today generally ascribed to the specific mobility of the screw dislocations with Burgers vectors of the type $a/2\langle 1\,1\,1\rangle$ below T_0. Conversely non-screw dislocations possess a planar core and are therefore considerably more mobile than screw dislocations. Because of their complicated core structure the screw dislocations exhibit a high Peierls stress. After low temperature strain bcc metals and alloys principally contain long screw dislocations of different $a/2\langle 1\,1\,1\rangle$

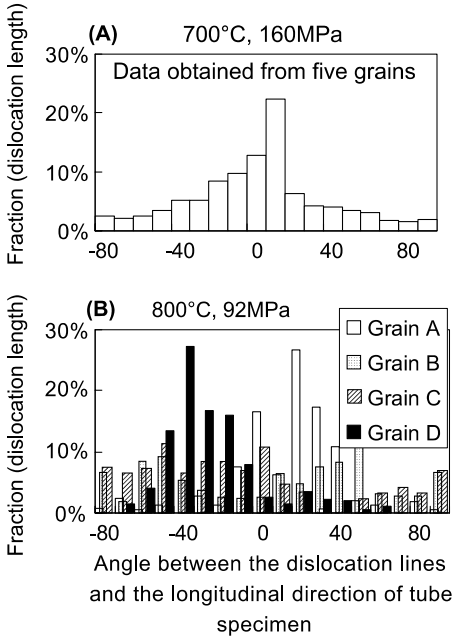

Fig. 4. The plots of dislocation length distribution as a function of an angle between a longitudinal direction of creep tube and a direction along a dislocation line. (A) 700 °C and (B) 800 °C.

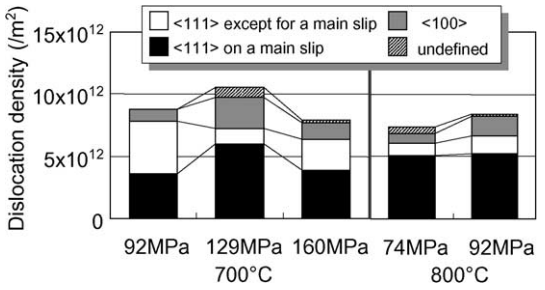

Fig. 5. Dislocation density distribution for the various types of dislocations in the creep-tested V–3Fe–4Ti–0.1Si alloy. The dislocation types were classified into four groups: (1) the ⟨1 1 1⟩ main slip; the slip dislocation oriented for optimum slip system during tests, (2) the ⟨1 1 1⟩ except for main slip; the slip dislocation oriented for different slip system from the optimum one, (3) ⟨0 0 1⟩ dislocation; the reaction dislocation produced by the intersection of dislocation movements, and (4) undefined dislocations.

Burgers vectors in homogeneous distributions without any excess of dislocations of one sign. However, with increasing temperature the difference between the mobilities of the screw and non-screw dislocations becomes progressively smaller as a result of thermal activation, so that the conditions become increasingly similar to those in fcc metals. Above the transition temperature, T_0, when the mobilities of screw and edge dislocations are comparable, there exist marked analogies in the deformation behavior of bcc and fcc metals [15]. The Peierls barrier in bcc metals for edge dislocation motion is comparable to that for screw dislocation motion above 700 °C (>$0.4T_m$). Hence a lot of dislocations can possess edge character after creep deformation. The plastic anisotropy during creep deformation is essential in vanadium alloys as well as other bcc metals and alloys at high temperatures around $0.5T_m$. The types of active slip system for edge dislocations in this alloy are considered to be $\langle 1\,1\,1\rangle\{1\,1\,0\}$ and $\langle 1\,1\,1\rangle\{1\,1\,2\}$ at high temperatures. Most of dislocation structures after thermal creep tests consist of $\langle 1\,1\,1\rangle$ edge dislocation in this study. Therefore these results conform well with the general dislocation theory at high temperatures mentioned above.

The preferential glide movement of dislocations in the V–3Fe–4Ti–0.1Si alloys causes the faster creep rate compared to V–4Cr–4Ti, and the recovery of dislocations is greater than in V–Cr–Ti alloys. The reason why the creep strength of the V–3Fe–4Ti–0.1Si alloy is lower than V–4Cr–4Ti is considered to be due to the difference of creep deformation mechanism, since the a V–4Cr–4Ti alloy forms the cell wall structure in spite of little difference in climb velocity and vacancy diffusion.

3.2. Microstructural examination for irradiation creep pressurized tube specimens

For the V–3Fe–4Ti–0.1Si alloys in this study, the effective strain and stress were 0.75%, 163 MPa and 0.91%, 165 MPa for specimens irradiated at 300 and 212 °C, respectively. After the irradiation, the surface of the creep tubes appeared to be darkened.

The microstructures of both an unstressed TEM specimen and a pressurized creep tube specimen irradiated at 300 °C are shown in Fig. 6. An arrow [H] inside the figure shows the hoop direction of the creep tube specimen. There are high densities of dislocations and defect clusters in both specimens. No precipitates can be seen in pressurized creep tube specimens irradiated at 212 and 300 °C. Fine contrasts are seen in unstressed TEM specimens but it was difficult to identify them as precipitates by diffraction and image techniques. In order to determine the Burgers vectors of the defect clusters, images with several reflections were taken in the same area. However the character of the defect clusters could not be determined because of the high densities of defect clusters.

In order to investigate the anisotropic formation of defect clusters in pressurized creep tube specimens, microstructures on several grains were taken, but no features typical of anisotropic microstructures of dislocation and defect clusters were observed. Fig. 7 shows the densities of defect clusters as a function of irradiation temperature. No significant difference of microstructures between unstressed and creep tube specimens was obtained. The densities of defect clusters in both specimens were the almost same and about 2×10^{22} clusters/m^3 at

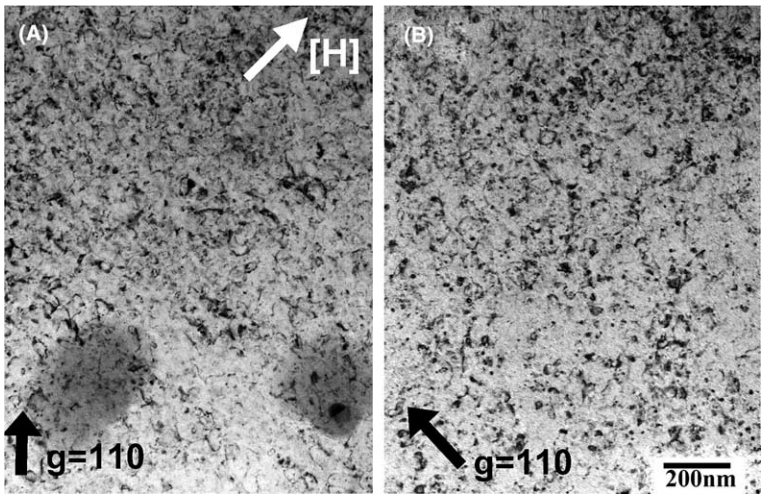

Fig. 6. Comparison of microstructures between unstressed and creep specimens of the V–3Fe–4Ti–0.1Si alloys irradiated at 300 °C in ATR-A1. (A) a pressurized creep tube specimens and (B) an unstressed TEM specimen. The arrow [H] in top in (A) indicates a hoop direction of the creep tube specimen.

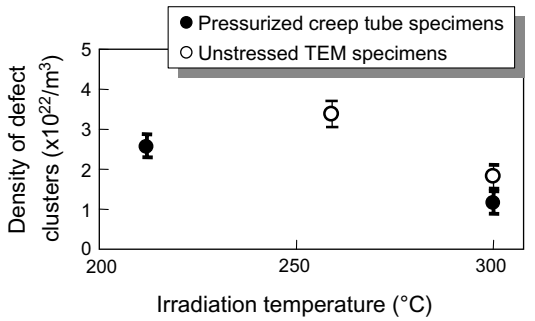

Fig. 7. Density of defect clusters in pressurized creep tubes and unstressed specimens.

temperatures from 212 to 300 °C. There is no anisotropic feature of the defect cluster formation in pressurized creep tube specimens during irradiation.

Since the high density of fine defect clusters and low temperature irradiation make the long-range diffusion of defects difficult, the difference in microstructural evolution between the stressed and unstressed specimens under irradiation was not apparent. Even though the diametric strains of unstressed specimens were for V–4Cr–4Ti alloys, the swelling of the unstressed V–4Cr–4Ti alloy is not considered to be much different from that of unstressed V–3Fe–4Ti–0.1Si alloys in the same irradiation condition in this study. The amount of swelling for the unstressed V–4Cr–4Ti alloys was 0.05% and 0.11% for the specimens irradiated at 212 and 300 °C, respectively. However, the effective strains in the creep specimens at 212 and 300 °C were about 0.75% and 0.91%, respectively. The amount of creep strain was much larger than that of volume expansion in unstressed specimens and quite large compared with ferritic steel and other alloys [2]. The origin for the enormous creep deformation in the creep specimens is still not identified from the microstructural observation using TEM. The dense defect clusters with a nano-scale size, such as microvoids, invisible interstitial clusters or impurity-titanium complexes may cause the creep strain rate and volume expansion during irradiation. However it is not clear why the fine defect structures are induced in stressed environment at low temperature. This is the future problem that must be studied more in detail.

4. Conclusions

Microstructural examinations for thermal creep and irradiation creep specimens of the V–3Fe–4Ti–0.1Si alloys were performed.

No anisotropic defect cluster formation was observed in pressurized creep tubes irradiated in ATR-A1 at temperatures from 212 to 300 °C. The cause for the large creep strain rate in creep specimens was not clear, as there was little difference in microstructural evolution between unstressed TEM specimens and pressurized creep tube irradiated in ATR-A1.

The type of creep deformation mechanism for V–3Fe–4Ti–0.1Si alloys was a dislocation glide creep controlled by solid solution strengthening. The formation of dislocation structures was caused by a large number of slip dislocations oriented for optimum slip.

Acknowledgement

The authors would like to express their thanks to Professor S. Tsurekawa of Tohoku University for using the SEM–EBSP/OIM system and Mr T. Matsuzaki for his help in the SEM–EBSP/OIM experiment. This work was partly supported by JUPITER program (Japan-USA Program of Irradiation Test for Fusion Research).

References

[1] R.J. Kurtz, K. Abe, V.M. Chernov, V.A. Kazakov, G.E. Lucas, H. Matsui, T. Muroga, G.R. Odette, D.L. Smith, S.J. Zinkle, J. Nucl. Mater. 283–287 (2000) 70.
[2] A. Kohyama, Y. Kohno, K. Asakura, M. Yoshino, Mater. Trans. JIM 34 (1993) 1061.
[3] R.J. Kurtz, M.L. Hamilton, J. Nucl. Mater. 283–287 (2000) 628.
[4] K. Abe, A. Kohyama, C. Namba, F.W. Wiffen, R.H. Jones, J. Nucl. Mater. 258–263 (1998) 2075.
[5] H. Tsai, H. Matsui, M.C. Billone, R.V. Strain, D.L. Smith, J. Nucl. Mater. 258–263 (1998) 1471.
[6] K. Fukumoto, H. Matsui, H. Tsai, D.L. Smith, J. Nucl. Mater. 283–287 (2000) 492.
[7] H. Matsui, H. Nakajima, Sci. Rep. RITU A 35 (2) (1991) 196.
[8] K. Fukumoto, T. Morimura, T. Tanaka, A. Kimura, K. Abe, H. Takahashi, H. Matsui, J. Nucl. Mater. 239 (1996) 170.
[9] K. Fukumoto, Y. Yan, H. Tsai, D.L. Smith, H. Matsui, in: S. Hanada et al. (Ed.), Proceedings of the 4th Pacific Rim International Conference on Advanced Materials and Processing, 2001, p. 1319.
[10] H. Tsai, T.S. Bray, H. Matsui, M.L. Grossbeck, K. Fukumoto, J. Gazda, M.C. Billone, D.L. Smith, J. Nucl. Mater. 283–287 (2000) 362.
[11] T. Muroga, T. Nagasaka, A. Iiyoshi, A. Kawabata, S. Sakurai, M. Sakata, J. Nucl. Mater. 283–287 (2000) 711.
[12] K. Fukumoto, T. Yamamoto, N. Nakao, S. Takahashi, H. Matsui, J. Nucl. Mater. 307–311 (2002) 610.
[13] E.R. Gilbert, L.D. Blackburnm, J. Eng. Mater. Tech. ASME. Trans (1977) 168.
[14] J.W. Edington, R.E. Smallman, Acta. Met. 12 (1964) 1313.
[15] A. Luft, Prog. Mater. Sci. 35 (1991) 97.